Acta Cryst. (1990). A46, 263-270

Accurate Structure Analysis by the Maximum-Entropy Method

BY MAKOTO SAKATA AND MASUMI SATO

Department of Applied Physics, Nagoya University, Furo-cho, Chikusa-ku, Nagoya, Japan 464-01

(*Received* 4 *August* 1989; *accepted* 3 *November* 1989)

Abstract

The electron-density map of an Si crystal is drawn by the maximum-entropy method (MEM) with 30 structure factors which were determined very accurately on an absolute scale by the *Pendellösung* method [Saka & Kato (1986). *Acta Cryst.* A42, 469-478]. It is shown that the following three beneficial points arise from the use of the MEM for accurate structure analysis. Firstly, a precise electron-density map can be obtained; the existence of bonding electrons is clearly visible in the maximum-entropy map, even though no forbidden reflections are included in the analysis. The structure factors calculated from the maximum-entropy map for the 222 and the 442 forbidden reflections show good agreement with those measured by different experiments. The final R factor was 0·05% as a consequence of the high accuracy of the measured structure factors. Secondly, there is no need to seek a better structural model which could be a complicated and time-consuming process in accurate structure analysis. Thirdly, the resolution of the maximum-entropy map is much higher than that of the map drawn by conventional Fourier transformation. It is also found in the case of silicon that phase information is not absolutely necessary because exactly the same density-distribution map can be obtained without any phase information as the map drawn with all the phase information.

1. Introduction

The maximum-entropy method (MEM) provides us with the least-biased deduction which is compatible with certain given information. There have been many theoretical studies (Narayan & Nityanada, 1982; Wilkins, Varghese & Lehmann, 1983; Livesey & Skilling, 1985; Navaza, 1985, 1986; Bricogne, 1988) to apply the method to problems in crystallography and, in particular, to Fourier inversion. There are many cases in crystallography which involve Fourier inversion. We here limit our study to the Fourier inversion from crystal structure-factor data to an estimate for the electron-density distribution of a crystal.

In principle, an infinite number of Fourier coefficients are needed to perform a Fourier inversion without any ambiguity. It is, however, simply not possible to satisfy this condition experimentally. Conventionally, Fourier inversion is performed by using a limited number of Fourier coefficients obtained by experiment and ignoring experimental errors. This procedure implicitly means that all the missing Fourier coefficients are set to zero. From the viewpoint of the maximum-entropy method, this is a highly biased assumption as to the missing information. There is no reason why all the missing structure factors have to be set to zero, simply because the experiment to measure them cannot be or was not carried out.

Through the many theoretical studies on the MEM, its potential usefulness has now been recognized to treat various problems in crystallography, such as the phase problem (Piro, 1983; Podjarny, Moras, Navaza & Alzari, 1988). There are, however, only a few examples for which MEM has actually been applied (Wei, 1985; Gull, Livesey & Sivia, 1987), particularly in the field of accurate structure analysis. The present position is far from providing a proper understanding of the usefulness and the practical problems of applying the MEM to accurate structure analysis. Under these circumstances, we investigated the capability of the MEM in the field of accurate structure analysis from the practical viewpoint, and in particular to investigate how precise a density-distribution map is obtained when the available structure-factor information is limited.

Saka & Kato (1986) measured the X-ray structure factors of Si for 30 net planes by the *Pendellösung* method. In this method, the period of X-ray field oscillation which is proportional to the magnitude of the structure factor is measured, instead of the ordinary integrated intensity measurement of Bragg reflections. For this reason, the *Pendellösung* method is claimed to have the highest accuracy for the measurement of X-ray structure factors. It enables one to measure X-ray structure factors on an absolute scale. For the same reason, however, it is very difficult to measure the so-called forbidden reflection such as 222 or 442 by this method. In fact, Saka & Kato (1986) did not measure any forbidden reflections.

The forbidden reflections of Si arise from the asphericity of the electron-density distribution owing to the bonding electrons and/or anharmonic thermal vibrations. At room temperature, most of the contribution comes from the bonding electrons (Keating,

0108-7673/90/040263-08$03.00

Nunes, Batterman & Hastings, 1971). The existence of the bonding-electron distribution affects not only the forbidden reflections but also all the Bragg reflections, although the contribution could be very small. Therefore, the information on the bonding-electron density must be included in all the structure factors of Si to some extent if they are determined to high accuracy. However, it is not known how to extract this information. Without the information on the forbidden reflections, the bonding-electron density cannot be visualized by conventional Fourier syntheses. Indeed, in order to calculate the bonding charge, Saka & Kato (1986) borrowed the values of the 222 and 442 reflections from other sources (Fehlman & Fujimoto, 1975; Trucano & Batterman, 1972), the accuracy of which is not as high as that of Saka and Kato's measurement.

The best deduction should enable us to extract all the information which is contained in the observed data. It is a challenge to tackle this problem. Some results concerning this problem obtained *via* the MEM are shown in this paper.

2. Theory

There are a few variations of the formalism of the MEM as applied to the Fourier inversion problem, *e.g.* Gull & Daniel (1978), Collins (1982), Wilkins, Varghese & Lehmann (1983). Since in essence these are the same, there should be no significant difference in the final result for these formalisms. In this study, we follow basically Collins's formalism. There is no particular reason for this selection except that it has an explicit formulation for the actual electron density rather than the normalized density.

Collins's formalism is based on the entropy expression, S, obtained by Jaynes (1968):

$$S = -\sum_{\mathbf{r}} \rho'(\mathbf{r}) \ln [\rho'(\mathbf{r})/\tau'(\mathbf{r})]. \quad (1)$$

The probability $\rho'(\mathbf{r})$ and prior probability $\tau'(\mathbf{r})$ are connected with the actual electron density by

$$\rho'(\mathbf{r}) = \rho(\mathbf{r})/\sum_{\mathbf{r}} \rho(\mathbf{r}) \quad (2)$$

$$\tau'(\mathbf{r}) = \tau(\mathbf{r})/\sum_{\mathbf{r}} \tau(\mathbf{r}) \quad (3)$$

where $\rho(\mathbf{r})$ is the electron density at a certain pixel $\mathbf{r}$ and $\tau(\mathbf{r})$ is the prior density for $\rho(\mathbf{r})$.

We introduce two types of weak constraints as given information; one is for phase-known structure factors and the other is for phase-unknown structure factors.

$$C_1 = (1/N_1) \sum_{\mathbf{k}} |F_{\rm cal}(\mathbf{k}) - F_{\rm obs}(\mathbf{k})|^2/\sigma^2(\mathbf{k}) \quad (4)$$

$$C_2 = (1/N_2) \sum_{\mathbf{k}} ||F_{\rm cal}(\mathbf{k})| - |F_{\rm obs}(\mathbf{k})||^2/\sigma^2(\mathbf{k}) \quad (5)$$

where N_1 and N_2 are the number of reflections for phase-known and phase-unknown structure factors, respectively, $F_{\rm obs}(\mathbf{k})$ is the observed structure factor for reflection $\mathbf{k}$, $\sigma(\mathbf{k})$ the standard deviation of $F_{\rm obs}(\mathbf{k})$, and $F_{\rm cal}(\mathbf{k})$ is the calculated structure factor given as

$$F_{\rm cal}(\mathbf{k}) = V \sum_{\mathbf{r}} \rho(\mathbf{r}) \exp(-2\pi i \mathbf{r}.\mathbf{k}), \quad (6)$$

where V is the unit-cell volume. The expected value for C_1 and C_2 is 1. The sums in (4) and (5) are taken over the set of points for which the phase-known and phase-unknown structure-factor data are measured. We use Lagrange's method of undetermined multipliers to constrain C_1 to be unity while we maximize the entropy. Then we have

$$Q(\lambda_1, \lambda_2) = -\sum_{\mathbf{r}} \rho(\mathbf{r}) \ln [\rho(\mathbf{r})/\tau(\mathbf{r})] - (\lambda_1/2)C_1 - (\lambda_2/2)C_2, \quad (7)$$

where λ_1 and λ_2 are Lagrange multipliers. By setting

$$\partial Q(\lambda_1, \lambda_2)/\partial \rho(\mathbf{r}) = 0 \quad (8)$$

and using some approximations given by Collins (1982), we have

$$\begin{aligned}\rho(\mathbf{r}) = \exp[\ln \tau(\mathbf{r}) &+ (\Lambda_1/N_1) \sum [1/\sigma^2(\mathbf{k})] \\ &\times \{F_{\rm obs}(\mathbf{k}) - F_{\rm cal}(\mathbf{k})\} \exp(-2\pi i \mathbf{k}.\mathbf{r}) \\ &+ (\Lambda_2/N_2) \sum [1/\sigma^2(\mathbf{k})] \\ &\times \{|F_{\rm obs}(\mathbf{k})| \exp[i\varphi(\mathbf{k})] - F_{\rm cal}(\mathbf{k})\} \\ &\times \exp(-2\pi i \mathbf{k}.\mathbf{r})],\end{aligned} \quad (9)$$

where

$$\Lambda_1 = \lambda_1 F_0, \qquad \Lambda_2 = \lambda_2 F_2 \quad (10)$$

and F_0 is equal to the number of electrons in a unit cell, Z. In the present study, we strictly confine the total number of electrons in the unit cell to be Z. Since all the structure factors are known on an absolute scale, this can be done in a straightforward way. When $F_{\rm obs}(\mathbf{k})$, $\sigma(\mathbf{k})$ and λ_i are given, we can obtain (9) which determines the MEM estimate for

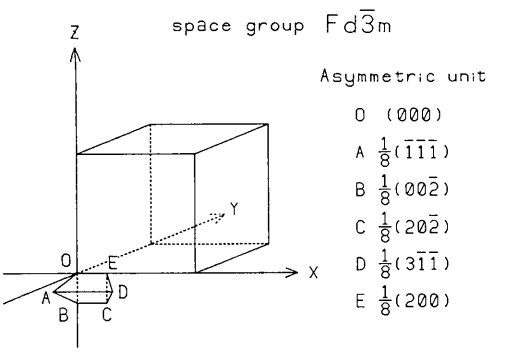

Fig. 1. Unit cell and asymmetric unit of space group $Fd\bar{3}m$.

the electron-density distribution, $\rho_{\rm MEM}(\mathbf{r})$. In practice, the value of $\rho_{\rm MEM}(\mathbf{r})$ has been solved numerically by an iterative procedure, starting from the uniform electron density.

In the present work, we use our knowledge of the space group. For this purpose, we calculate the electron density in the region of the minimum asymmetric unit. In the case of Si, of which the space group is $Fd\bar{3}m$, the asymmetric unit is written as $0 \le x \le \frac{1}{2}$; $0 \le y \le \frac{1}{8}$; $-\frac{1}{8} \le z \le \frac{1}{8}$; $y \le \min(\frac{1}{2}-x, x)$; $-y \le z \le y$ (*International Tables for Crystallography*, 1983). This asymmetric unit is shown in Fig. 1. After calculating the electron-density distribution of the minimum asymmetric unit by using (9), we can produce the electron-density distribution for the whole unit cell through the symmetry operations.

3. MEM density map

The computation time to obtain a three-dimensional MEM density-distribution map is sometimes enormous. As part of the effort to reduce the computation time, a fast Fourier transformation (FFT) was used to compute (6) in each iteration. For the FFT it is necessary to divide the unit cell into 2^n pixels. Here we computed $32\times32\times32$ or $64\times64\times64$ pixels by using $n = 5$ or 6.

The total number of electrons was always fixed at 112 which is equal to the number of electrons of 8 Si atoms in the unit cell. The initial electron density was set at $\tau(\mathbf{r}) = \langle\rho\rangle = 0{\cdot}699233$ (e Å^{-3}) for all pixels. This uniform electron-density distribution corresponds to the maximum-entropy state when no information on the structure factors is given. It is clear that no prejudice is included in the choice of the initial prior electron density. After the first iteration, $\tau(\mathbf{r})$ was replaced by the electron density obtained by that iteration.

3.1. *The phase-known analysis*

As a first step, we examined the MEM density map in the case where the phases of all the structure factors are known. These phases are easily obtained from the structure-factor calculation of diamond structure.

In this case, the iteration was continued until the condition $C_1 \le 1$ was attained. When this condition is attained, $\rho(\mathbf{r})$ is always very close to $\tau(\mathbf{r})$. This fact justifies the approximation which was used to derive (9). To clarify the procedure, the flow chart of the calculation is shown in Fig. 2. When the wrong λ_1 value is chosen, it always diverges as the iteration goes on. Whenever convergence is obtained, the same density-distribution map was obtained. In other words, the MEM density distribution does not depend on the choice of λ_1. This situation is exactly the same as for radio and X-ray astronomy fields (Gull & Daniel, 1978). It is also noticed that the larger λ_1, the quicker the convergence. In order to save computation time, we tried to find the largest λ_1 value which can lead to convergence.

It is convenient to show the various density distributions in the (110) plane, since the covalent bond is expected in this plane. The precise region for plotting the electron-density distribution in this plane and the atomic positions are shown in Fig. 3.

In Fig. 4, the MEM density map obtained on the basis of Saka & Kato's data is shown (*a*) for the higher-density region and (*b*) for the lower-density region in the case of $64\times64\times64$ pixels. Firstly, it should be mentioned that the atomic positions are correct as seen in Fig. 4(*a*). Secondly, the electron flow of the covalent bond appears beautifully in Fig. 4(*b*) and the maximum of the bonding electrons exists between the two Si atoms.

For comparison, the electron-density map drawn by the conventional Fourier method using the same

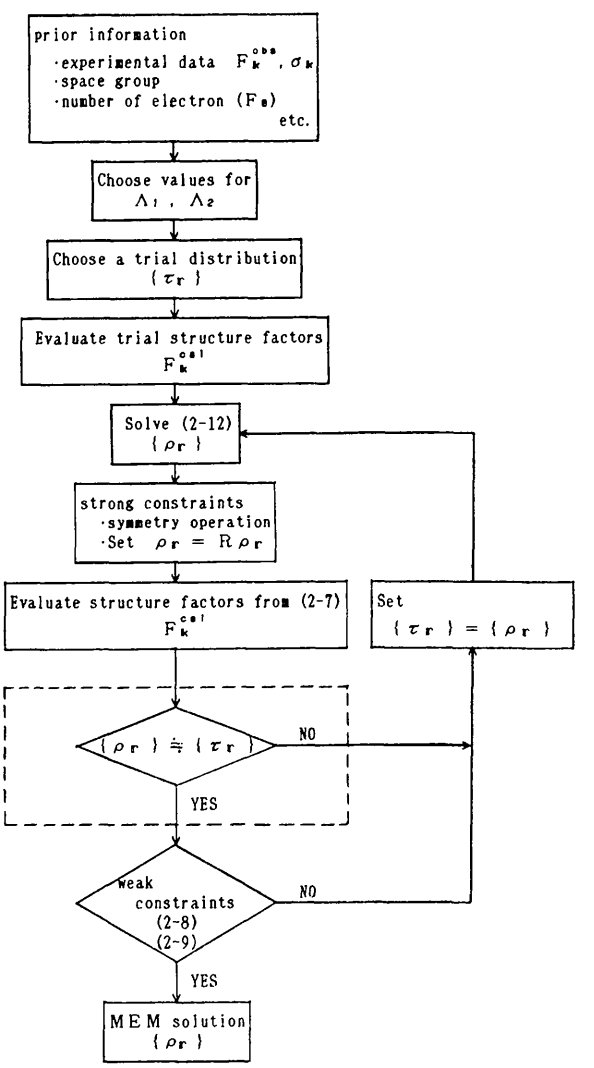

Fig. 2. Flow chart for the present calculation with the maximum-entropy method.

data set is shown in Fig. 5 with $32\times32\times32$ pixels. Although the atomic position is correct, there is no indication of bonding electrons in the figure. Furthermore, there is a negative-density region as a result of the termination of the Fourier sum. It has been pointed out that the MEM density distributions never have physically meaningless negative density (Gull & Daniel, 1978; Wilkins, Varghese & Lehmann, 1983). Another big difference between the two maps is the peak height of the density at the atomic position. The peak height in the MEM density map is 208 e $Å^{-3}$ and that of the conventional direct Fourier map is 96 e $Å^{-3}$, *i.e.* the peak height in the MEM density map is more than twice that of the conventional Fourier map. This is clear evidence that the MEM is superior to the conventional direct Fourier method, concerning the resolution of the density-distribution map obtained. It will be discussed in § 4 in more detail.

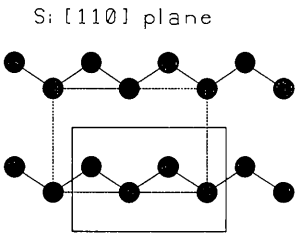

Fig. 3. Schematic diagram of the Si (110) plane. In Figs. 4, 5 and 7, the electron-density distribution of the area surrounded by the solid line is shown.

The observed, $F_{obs}(\mathbf{k})$, and the calculated, $F_{cal}(\mathbf{k})$, structure factors from MEM density distribution are listed in Table 1. As a result of the high accuracy of the measurement, the agreement is excellent. Since the iteration was continued until the condition $C_1 \leq 1$ was achieved, the overall agreement is determined by the e.s.d.'s of the structure factors. It is, therefore,

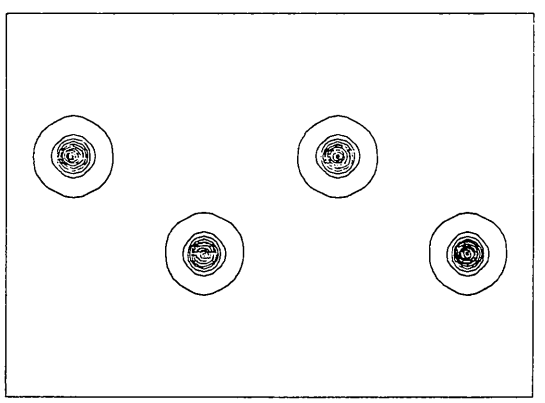

(*a*)

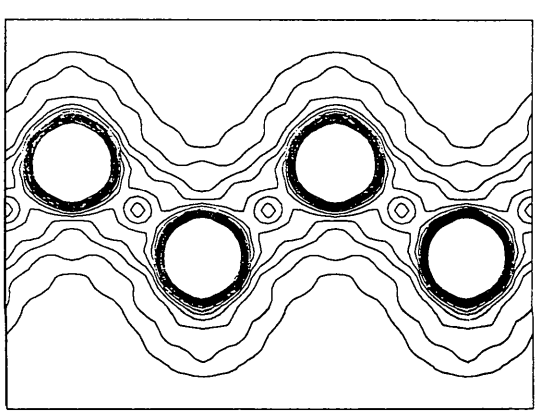

(*b*)

Fig. 4. The contour map of the electron-density distribution on the Si (110) plane deduced by the maximum-entropy method from Saka & Kato's data (*a*) for higher-density region and (*b*) for lower-density region. The contour lines (e $Å^{-3}$) are drawn from 1·50 to 201·50 with 20·0 intervals in (*a*) and from 0·1 to 1·5 with 0·1 intervals in (*b*). In the calculation, the unit cell is divided into $64\times64\times64$ pixels.

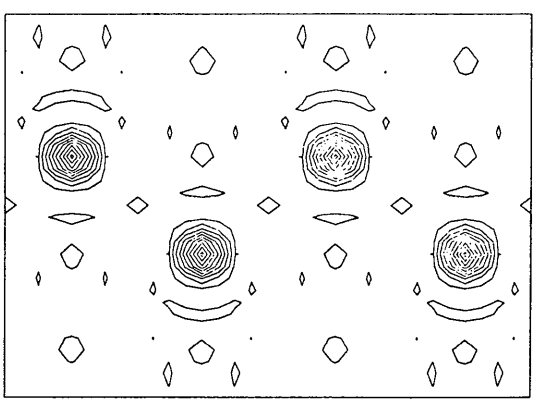

(*a*)

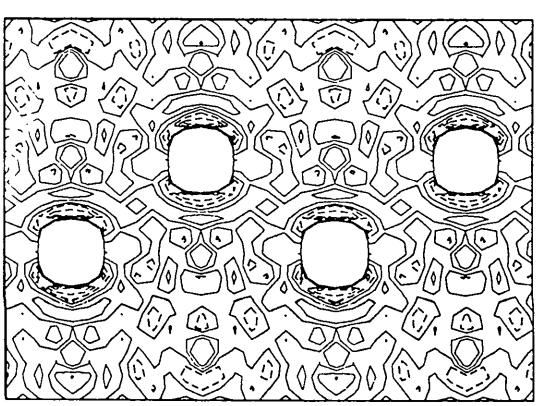

(*b*)

Fig. 5. The contour map of the electron-density distribution on the Si (110) plane calculated by the conventional direct Fourier method using Saka & Kato's data (*a*) for the higher-density region and (*b*) for the lower-density region. The contour lines (e $Å^{-3}$) are drawn from 1·6 to 91·6 with 10·0 intervals in (*a*) and from −2·40 to 1·6 with 0·8 intervals in (*b*). The negative-density region in (*b*) is drawn with dotted line.

Table 1. *The observed structure factors of* Si *by Saka & Kato* (1986) *and calculated structure factors from the density distribution obtained by the maximum-entropy method*

The phase is added for Saka & Kato's data, since there is no ambiguity of the determined phase.

h	k	l	F_{obs}	F_{cal}
0	0	0	—	112·0000
1	1	1	−60·1312	−59·9391
2	2	0	−67·3432	−67·5070
1	1	3	−43·6336	−43·6146
4	0	0	−56·2344	−56·2169
3	3	1	38·2239	38·2215
4	2	2	49·1056	49·0980
3	3	3	32·8329	32·8345
5	1	1	32·9410	32·9463
4	4	0	42·8848	42·8816
5	3	1	28·8143	28·8156
6	2	0	37·5872	37·5681
5	3	3	−25·3568	−25·3580
4	4	4	−33·1760	−33·1807
5	5	1	−22·4221	−22·4215
7	1	1	22·3712	22·3727
6	4	2	−29·4208	−29·4217
5	5	3	−19·9755	−19·9739
7	3	1	−19·8986	−19·8990
8	0	0	26·2272	26·2284
7	3	3	−17·8298	−17·8296
6	6	0	−23·4832	−23·4852
8	2	2	−23·4840	−23·4841
5	5	5	15·9784	15·9776
7	5	1	−15·9795	−15·9789
8	4	0	−21·1496	−21·1503
7	5	3	14·4295	14·4292
9	1	1	−14·4584	−14·4582
6	6	4	19·1256	19·1261
8	4	4	17·4384	17·4386
8	8	0	12·4112	12·4112

not necessary to express the overall agreement in the form of an R factor, which is defined as

$$R = \sum_{\mathbf{k}} |F_{obs}(\mathbf{k}) - F_{cal}(\mathbf{k})|^2 / |F_{obs}(\mathbf{k})|^2 \qquad (11)$$

and is commonly used in least-squares refinement. In this work, we use the R factor for convenience to allow easy comparison of MEM analysis with least-squares refinement. The value of the R factor is 0·0005 for the final MEM density map. It would be very difficult in a least-squares refinement to think of a structural model which would give such an excellent agreement. If we could not reach an R factor as low as this level in a least-squares refinement, the high accuracy of the measurement would be wasted. It should also be noticed that the peak height of the bonding electron is still much higher for the MEM density map, *i.e.* 0·7 e Å^{-3}, than that for the difference Fourier map calculated by Saka & Kato (1986) using 222 and 442 forbidden-reflection data from other sources (Fehlman & Fujimoto, 1975; Trucano & Batterman, 1972), *i.e.* 0·221 e Å^{-3}, which implies that the visibility of the small deformation of the electron-density distribution, like the bonding electrons, is much superior with the MEM than with the conventional Fourier method.

As far as the R factor is concerned, the density-distribution map of the conventional method yields a smaller value. Indeed, the calculated structure factors obtained from the density map of the conventional method are exactly the same as the observed ones, since the structure factors are calculated by the inverse Fourier transformation of the conventional density-distribution map which was initially obtained by the Fourier transformation of the observed structure factors. Therefore, the R factor is zero. However, the calculated structure factors for unmeasured Bragg reflections are all zero. This is very unlikely to be true in reality and shows the bias present in the conventional method of Fourier synthesis.

3.2. *The phase-unknown analysis*

As a second step, we attempted to calculate the MEM density map without using any phase information. The simple way to do this is to replace (4) by (5) as a constraint function. In this case, however, no convergence is reached no matter how λ_2 was chosen. In order to help the understanding of the situation, the value of the constraint function, C_2, is shown in Fig. 6 as a function of the number of iterations when (5) is used instead of (4). In the figure, the value of C_1 is also shown for the case of the phase-known analysis. It is understood that there is no sign of the convergence in the case of phase-unknown analysis. Therefore, we stopped the calculation which uses only (5) as a constraint.

In the present case, the phase of the structure factors are either 0 or 180°, because of the existence of the center of symmetry. Therefore, $F(hkl)$ is either $F(hkl) = +|F(hkl)|$ or $-|F(hkl)|$. Hence there are only two possibilities for the sign of a structure factor by MEM deduction if we select a particular reflection as a reference for a phase-known structure factor. We can calculate the contribution to the electron-density-distribution map for both cases. Incidentally, we

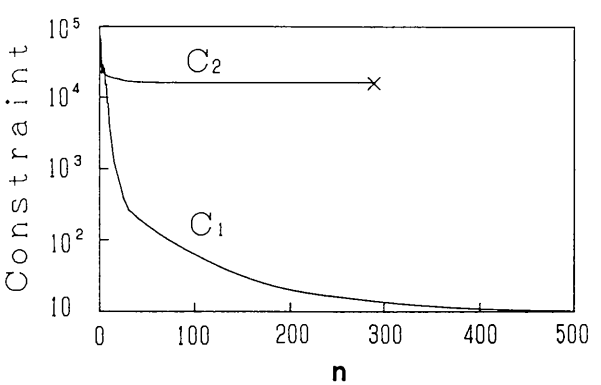

Fig. 6. The values of the constraint functions C_1 and C_2 against the number of iterations in the case of phase-known and phase-unknown analyses, respectively. In the case of the phase-unknown analysis, there is no sign of convergence. Hence the iteration was stopped at the point x.

selected $F(111)$ as the reference reflection. In this case, $F(111)$ is either +60·1312 or −60·1312. Using either of them, we obtained the density distribution shown in Fig. 7 as the two possibilities by phase-known analysis. They are identical except for the origin of the unit cell. There is no absolute criterion for the choice of the origin. Indeed, they actually represent the same structure. This happens in general in the case of structure determination with a center of symmetry.

After this procedure, we added the second constraint, (5), for the rest of the structure factors. We used the same value for λ_1 and λ_2. As a result, we obtained exactly the same MEM density distribution as that obtained by the phase-known analysis mentioned in § 3.1. Therefore, it can be said that the MEM density distribution of Si can be obtained without any phase information. The electron-density-distribution map shown in Fig. 4 is an *ab initio* solution by the MEM which was deduced from Saka & Kato's data. The map can be obtained without a structural model or any information on the phases of the structure factors.

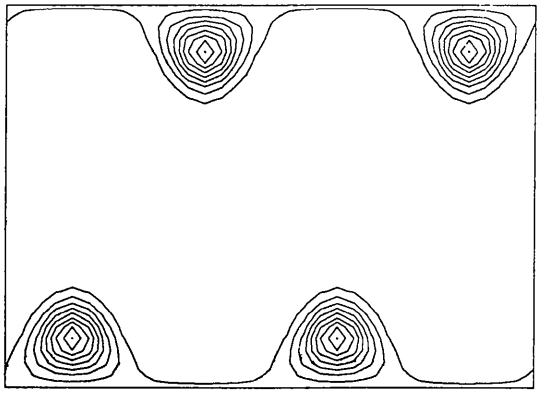

(*a*)

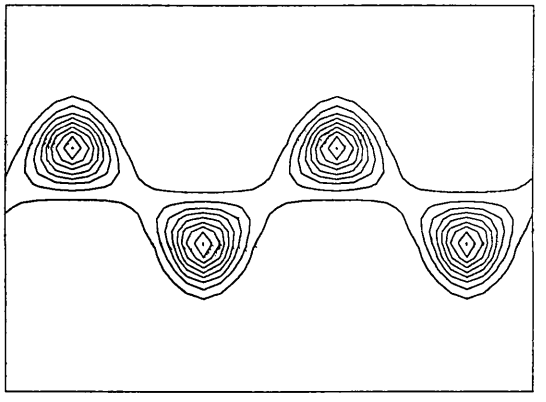

(*b*)

Fig. 7. The contour map of the electron-density distribution on the Si (110) plane using only one structure factor, $F(111)$. The phase of $F(111)$ is assumed (*a*) $F(111) = +\|F(111)\|$ and (*b*) $F(111) = -\|F(111)\|$. The contour lines are from 2·0 to 18·0 with 2·0 e Å^{-3} intervals.

4. High resolution of the MEM

In the field of the MEM analysis, the term super-resolution is sometimes used (Wilkins, Varghese & Lehmann, 1983) and refers to structural information inside the Shannon–Nyquist interval (Shannon, 1949). In the conventional method, the resolution is mainly restricted by termination errors in the Fourier sum, while the MEM tends to minimize termination errors.

The present analysis offers a very good demonstration of the high resolution achievable with the MEM. As pointed out in § 3.1, the peak height of the electron density at the atomic position is much higher in the MEM density map. This is because of the result of the high resolution of the MEM. This fact can be understood from the simple discussion presented below.

We calculated the electron density at the peak position using different numbers of structure-factor data. In the MEM analysis, we changed the number of data into 9 steps, which were 2, 5, 8, 11, 13, 18, 20, 25 and 28. For conventional Fourier synthesis, we used the calculated structure factors in order to extend the number of data to as many as we wished. In the structure-factor calculation, the temperature factor is fixed at the value quoted by Saka & Kato (1986). This value may not be valid for very high-order reflections, for which anharmonic thermal vibrations should be considered, but this effect does not affect the essence of the present discussion. In Fig. 8, the electron

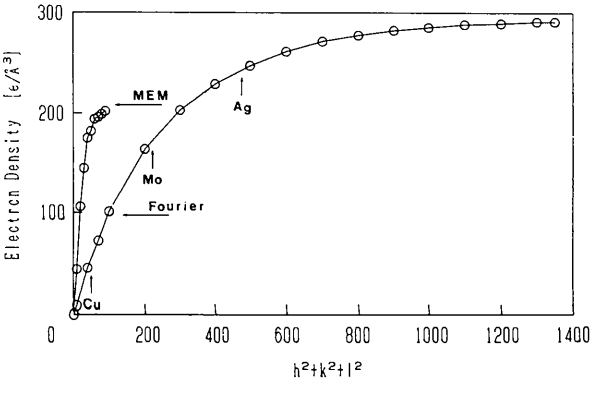

Fig. 8. The peak height of the electron-density distribution of Si is plotted against the number of structure-factor data used in the analysis. For the maximum-entropy method, Saka & Kato's data are used. For the conventional direct-Fourier method, the calculated structure factors are used in order to extend the number of data. In the structure-factor calculation, the temperature factor is fixed at the value quoted by Saka & Kato (1986). The vertical arrows labelled Cu, Mo and Ag represent the limit of the number of the data collected when Cu $K\alpha$, Mo $K\alpha$ and Ag $K\alpha$ radiations are used.

density at the peak position is plotted as a function of the maximum value of $h^2+k^2+l^2$ of the data used.

In conventional Fourier analysis, the peak height increases gradually as the number of data increases and reaches a nearly constant value, while, in the MEM, the increment is much steeper. In order to obtain a good estimate of the true electron density at a peak position, we have to know the higher-order anharmonicity which affects the very high-order reflections like 20,20,20 *etc.* It can, however, safely be said that the true electron density at the peak position is higher than that of the MEM density map. The conventional direct Fourier map shown in Fig. 5 has a much lower peak height than that of the MEM map because a limited number of structure factors is used in the Fourier synthesis. It can, therefore, be said that the electron density at a peak position obtained by the MEM analysis is much closer to the truth.

It should be mentioned here again that the very high electron density at the peak position in the MEM density map is not the result of any artificial procedures, since the MEM, in principle, tries to make the peak as low as possible so long as the constraint is satisfied.

5. Forbidden reflections

The MEM density map shown in Fig. 4 looks very satisfactory as seen in previous sections, although it is obtained without using any forbidden reflections. Since the MEM density-distribution map enables us to predict the values of unmeasured structure factors, we can compare the calculated structure factors from the MEM density map with some other experimental values for any reflections. It would be most interesting to do such a comparison for forbidden reflections. Fortunately, there have been quite a few experiments to determine the structure factors for forbidden reflections on an absolute scale.

For this purpose, the calculated structure factors from the present MEM density-distribution map are listed in Table 2 up to $h^2+k^2+l^2=300$, not only for forbidden reflections but also for all other unmeasured reflections by Saka & Kato (1986). Although it is possible to calculate the structure factors for further reflections, the $64\times64\times64$ pixels should not be precise enough for such higher-order reflections.

The structure factor $F(222)$ for silicon at room temperature has been measured by many authors by various experimental methods. They are conveniently summarized by Alkire, Yelon & Schneider (1982). We added our calculated values to them. They are shown in Table 3. At first glance, the prediction looks very reasonable. Although the predicted value is slightly higher than that of the recent experimental value by Alkire, Yelon & Schneider (1982), who claimed the highest accuracy, it is well within the range of the various experimental values. It is also noticed that the present value lies between two of the *Pendellösung*-fringe measurements which is the same experimental method as Saka & Kato's.

For the 442 and 622 forbidden reflections, many fewer measurements have so far been done than for the 222 reflection. They are tabulated in a recent work of Tischler & Batterman (1984). These experimental values are shown with the present values in Table 4.

Table 2. *The calculated structure factors from the MEM density-distribution map for unmeasured reflections by Saka & Kato* (1986)

h	k	l	F_{hkl}	h	k	l	F_{hkl}
2	2	2	1·5270	8	6	6	−10·8775
4	4	2	−0·0349	9	7	3	−7·4670
6	2	2	−0·0112	10	6	2	0·0493
6	4	4	−0·0126	8	8	4	−10·0092
6	6	2	0·0121	7	7	7	−6·8645
8	4	2	−0·0130	10	6	4	−9·2547
9	3	1	−13·0103	9	7	5	−6·3342
7	7	1	11·9035	9	9	1	−5·9879
9	3	3	11·8179	8	8	6	−0·0664
7	5	5	11·8539	10	8	2	−7·9477
10	2	0	−15·7866	9	9	3	−5·4320
8	6	2	15·7732	10	6	6	−0·0484
9	5	1	10·7391	9	7	7	4·8625
7	7	3	10·7586	10	8	4	−0·0436
10	2	2	0·0220	9	9	5	4·5386
6	6	6	0·0732	8	8	8	6·0861
9	5	3	9·8459	10	10	0	−5·9286
8	6	4	0·0510	10	8	6	5·7022
10	4	2	13·1099	10	10	2	−0·0021
7	7	5	−8·8417	9	9	7	3·6463
9	7	1	8·3286	10	10	4	5·0182
9	5	5	−8·1466	10	8	8	0·0485
8	8	2	0·0354	10	10	6	0·0411
10	4	4	0·0387	9	9	9	−2·6627
10	6	0	11·0482	10	10	8	−3·2102
				10	10	10	0·0299

Table 3. *Values of the structure factor $F(222)$ for silicon at room temperature*

Reference	$F(222)$
Hewat, Prager, Stephenson & Wagenfeld (1969)	0·88
Aldred & Hart (1973)	1·35 ± 0·04
DeMarco & Weiss (1965)	1·44 ± 0·08
Alkire, Yelon & Schneider (1982)	1·456 ± 0·008
Roberto & Batterman (1970)	1·46 ± 0·04
Jennings (1969)	1·48 ± 0·03
Fujimoto (1974)	1·50 ± 0·015
Present work (calculated value)	1·527
Colella & Merlini (1966)	1·54
Renninger (1960)	1·55
Fehlman & Fujimoto (1975)	1·65 ± 0·03
Göttlicher, Kuphal, Nagorsen & Wölfel (1959)	1·78

Table 4. *Values of the structure factors $F(442)$ and $F(622)$ for silicon at room temperature*

Reference	$F(442)$	$F(622)$
Trucano & Batterman (1972)	−0·035 ± 0·002	
Mills & Batterman (1980)	−0·042 ± 0·003	±0·005 ± 0·004
Tischler & Batterman (1984)	−0·0370 ± 0·0023	+0·0088 ± 0·0011
Present work (calculated values)	−0·0349	−0·0112

For the 442 reflection, the agreement between the present value and the three experimental values is extremely good. It is surprising to see that the simple MEM deduction is able to predict correctly such a small value for the structure factor.

For the 622 reflection, there is excellent agreement between the present value and two other experimental values for the magnitude of the structure factor. However, the calculated phase of the structure factor is opposite to the experimentally determined phase by Tischler & Batterman (1984). This disagreement is probably due to the limit of the present MEM deduction. If one remembers that the magnitude of $F(622)$ is less than 1% of that of the 222 forbidden reflection, such a limitation would be bearable. An improvement of the agreement between these two values may be made if we could increase the pixel number to $128 \times 128 \times 128$ in the MEM analysis, since the very small value of a structure factor like that for the 622 reflection may be affected significantly by the number of pixels used.

Tischler & Batterman (1984) have also determined the values of $F(442)$ and $F(622)$ for germanium including their phases. They found that the phase of the germanium 442 structure factor is opposite to that of silicon, while the phase of the 622 structure factor is the same for germanium and silicon. In this context, it would be very interesting to draw a very precise electron-density distribution of germanium and to find out where such a difference originates.

6. Concluding remarks

The accurately determined structure factors for Si obtained by the *Pendellösung* method include valuable information about the detail of the electron-density distribution such as the bonding electron density even if the forbidden reflections are excluded, whereas the conventional method of Fourier analysis fails to extract such information properly. On the other hand, the MEM enables us optionally to treat the information in the structure-factor data.

The MEM will be very useful in accurate structure analysis, because it is a model-free analysis, it can yield very high resolution on a density map provided the data are sufficiently accurate and it may work without phase information.

We thank Professor J. Harada for his critical reading of the manuscript. All the computations in this work were done at the Computer Center of Nagoya University which is gratefully acknowledged by the authors.

References

ALDRED, P. J. E. & HART, M. (1973). *Proc. R. Soc. London Ser. A*, **332**, 223-238.

ALKIRE, R. W., YELON, W. B. & SCHNEIDER, J. R. (1982). *Phys. Rev. B*, **26**, 3097-3104.

BRICOGNE, G. (1988). *Acta Cryst.* A**44**, 517-545.

COLELLA, R. & MERLINI, A. (1966). *Phys. Status Solidi*, **18**, 157-166.

COLLINS, D. M. (1982). *Nature (London)*, **298**, 49-51.

DEMARCO, J. J. & WEISS, R. J. (1965). *Phys. Rev.* **137**, A1869-A1871.

FEHLMAN, M. & FUJIMOTO, I. (1975), *J. Phys. Soc. Jpn*, **38**, 208-215.

FUJIMOTO, I. (1974). *Phys. Rev. B*, **9**, 591-599.

GÖTTLICHER, S., KUPHAL, R., NAGORSEN, G. & WÖLFEL, E. (1959). *Z. Phys. Chem. (Frankfurt am Main)*, **21**, 133-145.

GULL, S. F. & DANIEL, G. J. (1978). *Nature (London)*, **272**, 686-690.

GULL, S. F., LIVESEY, A. K. & SIVIA, S. (1987). *Acta Cryst.* A**43**, 112-117.

HEWAT, A. W., PRAGER, P., STEPHENSON, J. D. & WAGENFELD, H. (1969). A**25**, S213.

International Tables for Crystallography (1983). Vol. A, p. 686. Dordrecht: Reidel. (Present distributor Kluwer Academic Publishers, Dordrecht.)

JAYNES, E. T. (1968). *IEEE Trans. Syst. Sci. Cybern.* **SSC4**, 227-241.

JENNINGS, L. D. (1969). *J. Appl. Phys.* **40**, 5038-5044.

KEATING, D., NUNES, A., BATTERMAN, B. & HASTINGS, J. (1971). *Phys. Rev. B*, **4**, 2472-2478.

LIVESEY, A. K. & SKILLING, A. K. (1985). *Acta Cryst.* A**41**, 113-122.

MILLS, D. & BATTERMAN, B. W. (1980). *Phys. Rev. B*, **22**, 2887-2893.

NARAYAN, R. & NITYANADA, R. (1982). *Acta Cryst.* A**38**, 122-128.

NAVAZA, J. (1985). *Acta Cryst.* A**41**, 232-244.

NAVAZA, J. (1986). *Acta Cryst.* A**42**, 212-223.

PIRO, O. E. (1983). *Acta Cryst.* A**39**, 61-68.

PODJARNY, A. D., MORAS, D., NAVAZA, J. & ALZARI, P. M. (1988). *Acta Cryst.* A**44**, 545-551.

RENNINGER, M. (1960). *Z. Kristallogr.* **113**, 99-103.

ROBERTO, J. B. & BATTERMAN, B. W. (1970). *Phys. Rev. B*, **2**, 3220.

SAKA, T. & KATO, N. (1986). *Acta Cryst.* A**42**, 469-478.

SHANNON, C. E. (1949). *Proc. IRE*, **37**, 10-21.

TISCHLER, J. Z. & BATTERMAN, B. W. (1984). *Phys. Rev. B*, **30**, 7060-7066.

TRUCANO, P. & BATTERMAN, B. W. (1972). *Phys. Rev. B*, **6**, 3659-3666.

WEI, W. (1985). *J. Appl. Phys.* **18**, 442-445.

WILKINS, S. W., VARGHESE, J. N. & LEHMANN, M. S. (1983). *Acta Cryst.* A**39**, 47-60.